Acceptor Substrate Selectivity and Kinetic Mechanism of *Bacillus subtilis* TagA†

Yu-Hui Zhang,‡ Cynthia Ginsberg,‡,§ Yanqiu Yuan,‡,§ and Suzanne Walker*,‡

Department of Microbiology and Molecular Genetics, Harvard Medical School, Boston, Massachusetts 02115, and Department of Chemistry and Chemical Biology, Harvard University, Cambridge, Massachusetts 02138

Received May 2, 2006; Revised Manuscript Received July 7, 2006

ABSTRACT: Wall teichoic acids (WTAs) are anionic polymers that coat the cell walls of Gram-positive bacteria. Because they are essential for survival or virulence in many organisms, the enzymes involved in the biosynthesis of WTAs are attractive antibiotic targets. The first committed step in the WTA biosynthetic pathway in *Bacillus subtilis* is catalyzed by TagA, which transfers *N*-acetylmannosamine (ManNAc) to the C4 hydroxyl of a membrane-anchored *N*-acetylglucosaminyl diphospholipid (GlcNAc-pp-undecaprenyl, lipid I) to make ManNAc-β-(1,4)-GlcNAc-pp-undecaprenyl (lipid II). We have previously shown that TagA utilizes an alternative substrate containing a saturated $C_{13}H_{27}$ lipid chain. Here we use unnatural substrates and products to establish the lipid preferences of the enzyme and to characterize the kinetic mechanism. We report that TagA is a metal ion-independent glycosyltransferase that follows a steady-state ordered Bi-Bi mechanism in which UDP-ManNAc binds first and UDP is released last. TagA shares homology with a large family of bacterial glycosyltransferases, and the work described here should facilitate structural analysis of the enzyme in complex with its substrates.

WTAs[1] are anionic phosphate-rich polymers that are covalently linked to peptidoglycan in the cell walls of many Gram-positive bacteria, including pathogens such as *Staphylococcus aureus*, *Staphylococcus epidermis*, *Streptococcus pneumoniae*, *Enterococcus faecalis*, and *Listeria monocytogenes* (*1*). Although the functions of WTAs are poorly understood, they have been shown to be essential for survival in some organisms (*2*, *3*) and involved in virulence in others (*4*, *5*). For example, in *S. aureus*, WTAs are required for colonization of epithelial and endothelial tissues, and mutant strains lacking WTAs are poorly infective (*4*, *5*). Blocking WTA biosynthesis may thus be a promising strategy for combating Gram-positive bacterial infections. Structural and mechanistic information on enzymes involved in WTA biosynthesis could facilitate the identification of inhibitors, making it possible to evaluate the potential of the WTA pathway as a target for antimicrobial intervention.

WTAs from many different bacterial strains have been isolated and characterized, and they exhibit considerable structural variety. However, these polymers all share a general structure that can be divided into two parts: a *main chain* composed of repeating monomer units joined through phosphodiester linkages and a *linkage unit* that attaches the main chain to peptidoglycan (*1*). The most common main chain monomers are glycerol phosphate and ribitol phosphate (Figure 1). The linkage unit is highly conserved and consists of one to three glycerol phosphate (Gro-P) units attached to an *N*-acetylmannosaminyl β-(1,4)-*N*-acetylglucosaminyl [ManNAc-β-(1,4)-GlcNAc] disaccharide, which is anchored to peptidoglycan through a phosphodiester linkage to C6 of some of the *N*-acetylmuramoyl pentapeptide units (Figure 2) (*6*).

WTA biosynthesis has been studied most extensively in *Bacillus subtilis*, which is the major model organism for Gram-positive bacteria. The *tag* pathway for polyglycerol phosphate WTA synthesis in *B. subtilis* 168 is outlined in Figure 2 and serves as the paradigm for WTA biosynthesis in other organisms (*1*).

WTAs are assembled on an undecaprenyl "carrier lipid" anchored in the cytoplasmic membrane, then flipped across the membrane by an ABC-type transporter, and attached to peptidoglycan (*1*). The initial GlcNAc-pp-undecaprenyl membrane acceptor is formed by TagO, an enzyme that may also be involved in the synthesis of teichuronic acids and various minor teichoic acid polymers (*7*). Therefore, the first committed step in the WTA biosynthetic pathway in *B. subtilis* is catalyzed by TagA, a glycosyltransferase (Gtf) that forms a β-glycosidic linkage between *N*-acetylmannosamine (ManNAc) and the C4 hydroxyl of a membrane-anchored *N*-acetylglucosaminyl diphospholipid (GlcNAc-pp-undecaprenyl, lipid I), to give ManNAc-β-(1,4)-GlcNAc-pp-undecaprenyl (lipid II). Sequence homologies indicate that TagA is related to a family of uncharacterized glycosyltransferases involved in the biosynthesis of bacterial cell surface structures (*8*), including WecG, a UDP-*N*-acetyl-D-mannosaminuronic acid transferase involved in enterobacterial common antigen synthesis (*9*), and CpsF, a CMP-*N*-acetylneuraminic acid synthetase involved in capsular polysaccharide biosynthesis (*10*). These enzymes do not appear to resemble any Gtfs for which structural information is available (*11*−*14*). Therefore,

† This work was partially supported by NIH Grant A144854.

* To whom correspondence should be addressed. Tel: 617-496-0207. Fax: 617-496-0215. E-mail: suzanne_walker@hms.harvard.edu.

‡ Department of Microbiology and Molecular Genetics, Harvard Medical School.

§ Department of Chemistry and Chemical Biology, Harvard University.

[1] Abbreviations: WTA, wall teichoic acid; Gtf, glycosyltransferase; Gro-P, glycerol phosphate; Rbo-P, ribitol phosphate; GlcNAc, *N*-acetylglucosamine; ManNAc, *N*-acetylmannosamine; PP, pyrophosphate; lipid I, GlcNAc-pp-undecaprenyl; lipid II, ManNAc-GlcNAc-pp-undecaprenyl.

10.1021/bi060872z CCC: $33.50
Published on Web 08/18/2006

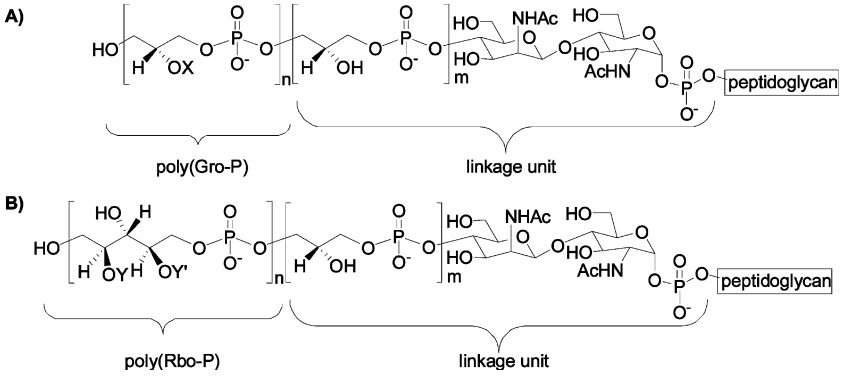

FIGURE 1: Representative wall teichoic acid structures. The polyol chains are usually modified with sugars, amino sugars, or D-alanyl esters (*1*). The type and extent of modification vary among bacterial strains and also depend on the bacterial environment. (A) Polyglycerol phosphate variants: *B. subtilis* 168, X = D-alanine/α-glucose/H; *S. epidermis* RP62A, X = D-alanine/α-glucose/α-glucose-6-*O*-alanine/α-GlcNAc. (B) Polyribitol phosphate variants: *S. aureus* H, Y = D-alanine and Y′ = α- or *β*-GlcNAc; *L. monocytogenes* serotype 1/2, Y = α-rhamnose and Y′ = α-GlcNac.

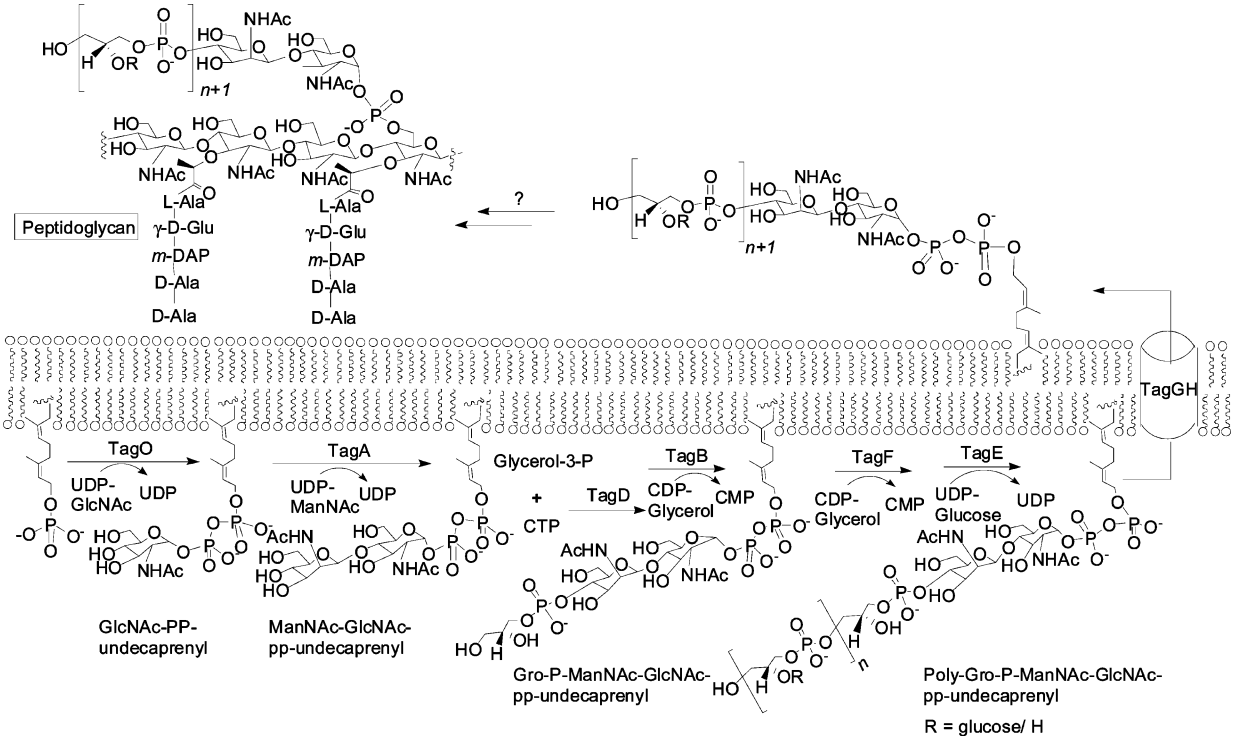

FIGURE 2: Polyglycerol phosphate WTA biosynthesis in *B. subtilis* 168. Different bacterial strains synthesize different main chain monomers, but synthesis of the linkage unit is largely conserved.

TagA is a potential target for antimicrobial agents as well as a model system for an uncharacterized family of Gtfs. Information on the kinetic mechanism of the enzyme may lay the groundwork for more detailed structural and mechanistic investigations.

We have recently reconstituted the activity of *B. subtilis* TagA in vitro using the synthetic substrate analogue GlcNAc-pp-$C_{13}H_{27}$ (*15*). This synthetic substrate contains a much shorter lipid chain than the natural substrate, which has a 55 carbon undecaprenyl "carrier" lipid that makes substrate isolation and kinetic studies of TagA challenging. Here we investigate the optimal reaction conditions and substrate preferences of *B. subtilis* TagA and then use this information in the kinetic characterization of the enzyme. We demonstrate that TagA follows an ordered Bi-Bi kinetic mechanism, where UDP-ManNAc binds first and the UDP product is released last. Information concerning the substrate preferences and kinetic mechanism of the enzyme should facilitate crystallization of TagA bound to substrate or product analogues and may help to guide efforts to obtain specific inhibitors of this enzyme.

MATERIALS AND METHODS

General Materials and Methods. All chemicals were purchased from Sigma-Aldrich and used without further purification except where otherwise noted. Reagent grade solvents were used and were further dried when necessary. ^{1}H NMR spectra were recorded on a Varian Inova 600 MHz spectrometer. Mass spectra (ESI) were recorded using an Agilent 1100 series LC/MSD instrument.

B. subtilis TagA was overexpressed, purified as described (*15*), and then stored at −80 °C as a 20% glycerol stock (20

mM Tris-HCl, pH 7.9, 200 mM imidazole, and 0.5 M NaCl). The enzyme concentration was calculated from the absorbance of the protein at 280 nm (denatured in 6 M guanidine hydrochloride) using the molar extinction coefficient of 40680 calculated for TagA. Lipid I analogues **1**−**5** (Figure 4) were prepared according to literature methods (*15*−*17*). The ^{1}H NMR spectrum of **1** was reported previously (*15*).

Lipid I analogue **2**: ^{1}H NMR (600 MHz, D_2O) δ 5.35 (dd, J = 3.2, 7.3 Hz, 1H), 5.32 (t, J = 7.0 Hz, 1H), 5.09−5.06 (m, 1H), 4.36−4.31 (m, 2H), 3.85 (dt, J = 3.2, 10.6 Hz, 1H), 3.79 (ddd, J = 2.3, 4.4, 10.0 Hz, 1H), 3.74 (dd, J = 2.3, 12.3 Hz, 1H), 3.68 (dd, J = 9.1, 10.6 Hz, 1H), 3.66 (dd, J = 4.4, 12.3 Hz, 1H), 3.40 (dd, J = 9.1, 10.0 Hz, 1H), 2.03−1.99 (m, 4H), 1.94 (s, 3H), 1.65 (s, 3H), 1.57 (s, 3H), 1.50 (s, 3H); ESI-MS calculated for $C_{18}H_{32}NO_{12}P_2$ [M^-], 516.1; found, 516.2.

Lipid I analogue **3**: ^{1}H NMR (600 MHz, D_2O) δ 5.35 (dd, J = 3.2, 7.3 Hz, 1H), 5.32 (t, J = 7.0 Hz, 1H), 5.09−5.06 (m, 2H), 4.36−4.31 (m, 2H), 3.85 (dt, J = 3.2, 10.6 Hz, 1H), 3.79 (ddd, J = 2.3, 4.4, 10.0 Hz, 1H), 3.74 (dd, J = 2.3, 12.3 Hz, 1H), 3.68 (dd, J = 9.1, 10.6 Hz, 1H), 3.66 (dd, J = 4.4, 12.3 Hz, 1H), 3.40 (dd, J = 9.1, 10.0 Hz, 1H), 2.03−1.99 (m, 4H), 1.98−1.96 (m, 4H),1.93 (s, 3H), 1.63 (s, 3H), 1.56 (s, 6H), 1.50 (s, 3H); ESI-MS calculated for $C_{23}H_{40}NO_{12}P_2$ [M^-], 584.2; found, 584.3.

Lipid I analogue **4**: ^{1}H NMR (600 MHz, D_2O) δ 5.38 (dd, J = 2.9, 7.0 Hz, 1H), 5.29 (t, J = 6.5 Hz, 1H), 5.02−4.95 (m, 3H), 4.36−4.34 (m, 2H), 3.85 (dt, J = 2.9, 10.6 Hz, 1H), 3.79 (ddd, J = 2.3, 4.4, 10.0 Hz, 1H), 3.74 (dd, J = 2.3, 12.3 Hz, 1H), 3.68 (dd, J = 9.1, 10.6 Hz, 1H), 3.66 (dd, J = 4.4, 12.3 Hz, 1H), 3.40 (dd, J = 9.1, 10.0 Hz, 1H), 2.00−1.89 (m, 8H), 1.93 (s, 3H), 1.86−1.82 (m, 4H), 1.59 (s, 3H), 1.53 (s, 3H), 1.48 (s, 3H), 1.45 (s, 6H); ESI-MS calculated for $C_{28}H_{48}NO_{12}P_2$ [M^-], 652.2; found, 652.2.

Lipid I analogue **5**: ^{1}H NMR (600 MHz, D_2O) δ 5.35 (dd, J = 3.2, 7.3 Hz, 1H), 5.30 (t, J = 6.7 Hz, 1H), 5.04−4.90 (m, 3H), 4.32−4.30 (m, 2H), 3.85 (dt, J = 3.2, 10.6 Hz, 1H), 3.79 (ddd, J = 2.3, 4.4, 10.0 Hz, 1H), 3.74 (dd, J = 2.3, 12.3 Hz, 1H), 3.68 (dd, J = 9.1, 10.6 Hz, 1H), 3.66 (dd, J = 4.4, 12.3 Hz, 1H), 3.40 (dd, J = 9.1, 10.0 Hz, 1H), 2.01−1.98 (m, 4H), 1.96−1.89 (m, 8H),1.92 (s, 3H), 1.60 (s, 3H), 1.54 (s, 3H), 1.52 (s, 6H), 1.45 (s, 3H); ESI-MS calculated for $C_{28}H_{48}NO_{12}P_2$ [M^-], 652.2; found, 652.3.

Enzymatic Synthesis of 5a. **5a** (Figure 4) was prepared from **5** using purified TagA. Compound **5** (3.2 mg) was dissolved in 1 mL of 1:1 CH_3OH-H_2O and added to 50 mL of TagA reaction buffer (50 mM Tris-HCl, pH 7.8, 250 mM NaCl, 100 mM imidazole, 10 mg of TagA), followed by 6.1 mg of UDP-ManNAc dissolved in 0.5 mL of H_2O. After 12 h at room temperature, LC/MS analysis showed almost 100% conversion to product. The crude reaction mixture was concentrated to ∼1 mL, 15 mL MeOH was added to recrystallize the salts, and the resulting mixture was filtered. The filtrate was concentrated, and the residue was dissolved in 300 μL of H_2O and purified over an Alltech High-Flow C18 Extract-Clean SPE column (60 Å, 100 mg, 1.5 mL). The disaccharide product was eluted with a gradient of 0−100% CH_3OH in 0.1% aqueous NH_4HCO_3 to obtain pure **5a** in quantitative yield (ESI-MS calculated for $C_{31}H_{53}N_2O_{17}P_2$ [M^-], 787.2; found, 787.4).

HPLC Assay. Reaction mixtures were analyzed using an Agilent 1100 series HPLC instrument with a binary pump and a standard autosampler. Each sample solution (20 μL) was injected on a Phenomenex Luna NH_2 column (3 μm, 150 × 4.6 mm) and eluted at a flow rate of 0.5 mL/min using a gradient of 50−100% solution B over 10 min, followed by a 12 min wash with 100% solution B (solution A, 20 mM sodium phosphate, pH 7.0, 10% acetonitrile; solution B, 20 mM sodium phosphate, pH 7.0, 10% acetonitrile, 1 M sodium chloride). UV peaks corresponding to UDP were measured at 260 nm and automatically integrated using the Agilent ChemStation data browser. To convert the measured peak areas to UDP concentrations, a calibration curve was constructed using known concentrations of UDP. Control experiments described in the text have established that UDP formation correlates with the extent of glycosyl transfer.

LC/MS Assay. Reactions were quenched with 15 μL of DMF containing 20 μM **4** as an internal standard. Mass spectrometric data were obtained on an Agilent 1100 series LC/MSD mass spectrometer equipped with a binary pump and a standard autosampler. Each sample solution (10 μL) was injected on an Agilent C18 column (5 μm, 250 × 4.6 mm) and eluted at a flow rate of 0.5 mL/min using a step gradient: 0−20% solution B over 8 min, 20−95% solution B over 1 min, and 95% solution B for 14 min (solution A, water; solution B, acetonitrile). The column temperature was set to 35 °C. The eluate was directed to waste for 10 min to flush the salts out of the system, after which the entire eluate was redirected into the ESI source of the quadruple mass spectrometer. The drying gas temperature and the spray voltage were kept at 350 °C and 3.0 kV, respectively. Selective ion monitoring (SIM) was used to detect ions of lipid II and internal standard **4**. The total ion chromatogram (TIC) peak area for each SIM ion was automatically integrated using the Agilent ChemStation data browser. The integrated peak areas of the product ion and the internal standard ion were used to calculate a peak area ratio (A_p/A_{is}). Calibration curves were constructed using known concentrations of the lipid II product and internal standard **4** and used to convert the lipid II concentration from the peak area ratio.

Preliminary Enzyme Assays. The pH dependence of TagA activity was measured at room temperature between pH 6.3 and pH 9.5 using Bis-Tris propane buffer (50 mM). The effects of NaCl, divalent metal ions, and EDTA on catalysis were determined in Tris-HCl buffer (50 mM, pH 7.8). Reactions were carried out in a total volume of 15 μL and contained 100 nM TagA, 250 mM NaCl, 100 μM UDP-ManNAc, and 100 μM **1**. Reaction rates were determined using the HPLC assay.

Enzyme Kinetics. Substrates and TagA were added at the indicated concentrations to a 15 μL reaction mixture containing 50 mM Tris, pH 7.8, and 250 mM NaCl. Compounds **1** and **2** were added to the reactions in water, and **3**−**5** were added in 1:1 H_2O-CH_3OH. Reactions were initiated by the addition of TagA and incubated at room temperature. To obtain initial rate data, incubation times were chosen so that there was less than 15% conversion to product. Reactions were quenched with 15 μL of DMF and centrifuged for 20 min at 14000*g* prior to analysis.

The values of $K_{m,app}$ and V_{max} for **1**−**5** were determined using the HPLC assay. Assays were carried out with [UDP-ManNAc] fixed at 600 μM (about three times K_m) because

of the limited supply of this synthetic substrate. For **3**−**5**, 10% DMSO was added to the reaction mixtures to ensure the solubility of the glycosyl acceptors. Preliminary experiments using substrate **1** have shown that DMSO concentrations up to 17% have a negligible effect on the activity of TagA (see Supporting Information).

For the mechanistic analysis, a 5 × 5 matrix of initial rate reactions was constructed with [UDP-ManNAc] at 25, 50, 100, 200, and 600 μM and [**3**] at 25, 50, 100, 200, and 500 μM. Rates were determined using the HPLC assay.

Product Inhibition Studies. The inhibition of TagA activity by UDP was determined using the LC/MS assay. For inhibition with respect to UDP-ManNAc, [**3**] was held at 100 μM, and UDP and UDP-ManNAc were added at the concentrations indicated in Figure 6A. For inhibition with respect to **3**, [UDP-ManNAc] was held at 100 μM, and UDP and **3** were added at the concentrations indicated in Figure 6B. Prior to analysis, all reactions were quenched with 15 μL of DMF containing 20 μM **4** as the internal standard.

To look at inhibition of TagA by **5a**, reaction rates were determined using the HPLC assay. For inhibition with respect to UDP-ManNAc, [**3**] was held at 200 μM, and **5a** and UDP-ManNAc were added at the concentrations indicated in Figure 7A. For inhibition with respect to **3**, [UDP-ManNAc] was held at 100 μM, and **5a** and **3** were added at the concentrations indicated in Figure 8A. Compound **5a** was added to the reactions in 1:1 MeOH−DMSO.

Data Processing. Initial rate data from the kinetic studies described were plotted as 1/(initial velocity) vs 1/(substrate concentration). The data were fit to the appropriate rate equations using the program Prism 4.0 (GraphPad software). K_m and k_{cat} values were determined by fitting the initial rates to the Michaelis−Menten equation (eq 1). Data conforming to a sequential mechanism were fit to eq 2. Data for competitive inhibition, noncompetitive inhibition, *I*-parabolic *S*-parabolic noncompetitive inhibition, and *I*-linear *S*-parabolic noncompetitive inhibition were fit to eqs 3, 4, 5, and 6, respectively.

$$v = VA/(K_m + A) \quad (1)$$

$$\frac{1}{v} = \frac{1}{V}\left[1 + \frac{K_a}{A} + K_b\left(1 + \frac{K_{ia}}{A}\right)\frac{1}{B}\right] \quad (2)$$

$$\frac{1}{v} = \frac{1}{V}\left[1 + K_a\left(1 + \frac{I}{K_{is}}\right)\frac{1}{A}\right] \quad (3)$$

$$\frac{1}{v} = \frac{1}{V}\left[1 + \frac{I}{K_{ii}} + K_a\left(1 + \frac{I}{K_{is}}\right)\frac{1}{A}\right] \quad (4)$$

$$\frac{1}{v} = a + bI + cI^2 + (d + eI + fI^2)\frac{1}{A} \quad (5)$$

$$\frac{1}{v} = a + bI + (d + eI + fI^2)\frac{1}{A} \quad (6)$$

In eqs 1−6, *A* and *B* are the concentrations of the reactants, *I* is the concentration of inhibitor, v and V represent initial and maximum velocities, respectively, K_a and K_b are Michaelis constants for *A* and *B*, K_{ia} is the inhibition constant for substrate A, and K_{is} and K_{ii} are the inhibition constants for the slope and the intercept, respectively.

RESULTS

Conditions for Optimal Activity of TagA. Preliminary experiments were carried out to determine suitable conditions for studying the kinetics of TagA. TagA showed optimal activity at pH 7.8 in Bis-Tris propane buffer (see Supporting Information), and the enzymatic activity proved to be sensitive to NaCl concentration, with the highest activity observed at 250 mM (Figure 3A). Because many enzymes that bind dinucleotide substrates require divalent, oxophilic cations such as Mg^{2+} or Mn^{2+}, we also examined the effects of these metal ions on the activity of TagA. Activity does not improve with the addition of Mg^{2+} or Mn^{2+} at concentrations up to 30 mM and does not decrease with the addition of EDTA (Figure 3). Therefore, TagA does not require Mg^{2+} or Mn^{2+} cations for activity.

Evaluation of Lipid I Analogues. The natural acceptor substrate for TagA contains a 55 carbon undecaprenyl chain. This substrate is difficult to isolate from bacterial membranes, and the undecaprenyl chain renders it insoluble in aqueous buffer, complicating kinetic studies of TagA activity. We previously demonstrated that TagA is able to utilize a synthetic substrate (**1**) containing a 13 carbon saturated chain (*15*). Here we investigate several additional substrate analogues to determine how sensitive TagA is to the structure of the lipid chain and to identify better substrates, if possible, for monitoring enzymatic activity. To this end, we synthesized lipid I analogues **2**−**5** (Figure 4) containing lipids of varying length and double bond geometry (*15*−*17*). Compounds **2**, **3**, and **5** contain *cis* double bonds like the natural substrate but vary in length from 10 to 20 carbons. Compound **4**, like compound **5**, contains 20 carbons, but the double bonds are *trans*.

Preliminary studies showed that TagA converts all of these lipid I analogues to products, so we determined the kinetic parameters for each acceptor using a HPLC assay that monitors formation of UDP to determine the reaction rate. To ensure that UDP production was the result of glycosyl transfer rather than hydrolysis, we first incubated UDP-ManNAc with TagA for 4 h in the absence of the acceptor. No UDP formation was detected by HPLC. We then determined the kinetic parameters of **1** at 600 μM UDP-ManNAc using the HPLC assay and LC/MS assay that directly monitors formation of the glycosylated lipid II product (see below and Materials and Methods for details). The values of $K_{m,app}$ and k_{cat} obtained for **1** using both assays were almost identical. These results show that UDP formation correlates directly with glycosyl transfer (see Supporting Information) and suggest that hydrolysis of the glycosyl donor does not occur to a significant extent in either the presence or absence of glycosyl acceptors.

Having established that validity of the HPLC assay for reporting on glycosyl transfer, we used it to measure the catalytic efficiencies of substrates **1**−**5** at 600 μM UDP-ManNAc. Substrates **4** and **5** showed substrate inhibition at concentrations above 100 and 300 μM, respectively, and only the initial rates of **1**, **2**, **3**, and **5** could be fit to the Michaelis−Menten equation (see Supporting Information). The $K_{m,app}$ and k_{cat} of **4** are crude estimates based on the first part of the reaction rate curve. The results (Table 1) show that **4**

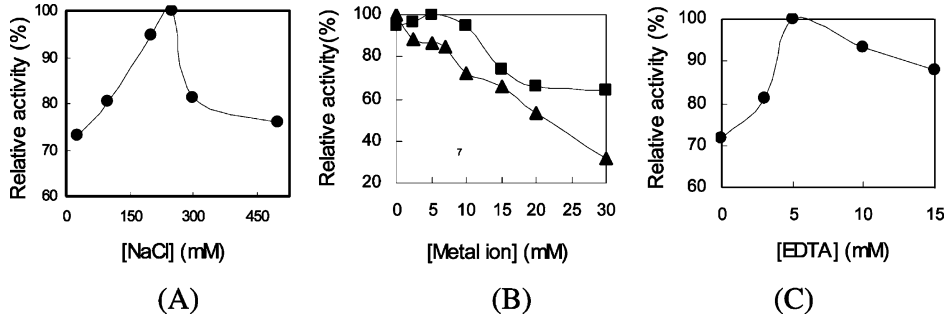

FIGURE 3: Effect of increasing concentrations of NaCl (A), Mn^{2+} (■) and Mg^{2+} (▲) ions (B), and EDTA (C) on TagA activity. Assays were carried out at 100 μM UDP-ManNAc, 100 μM lipid I analogue **1**, and 100 nM TagA.

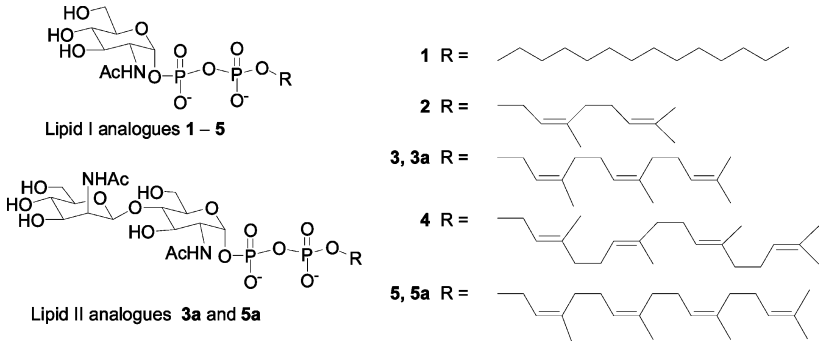

FIGURE 4: Lipid I and lipid II analogues described in the text.

Table 1: Apparent K_m and k_{cat} of Lipid I Analogues at 600 μM UDP-ManNAc

lipid I analogue	K_m (μM)	k_{cat} (min^{-1})	k_{cat}/K_m ($min^{-1}\,\mu M^{-1}$)
1	193 ± 34	551	2.85
2	258 ± 49	52	0.20
3	22 ± 10	835	3.67
4[a,b]	30	615	20.50
5[b]	35 ± 4	517	14.77

[a] Due to substrate inhibition above 100 μM, the $K_{m,app}$ of **4** is estimated as the substrate concentration at $^1/_2$ × highest observed rate. [b] The substrate range lower limit for **4** and **5** (25 μM) is close to the calculated K_ms, and the reported values may thus be *under*estimates. This does not affect the validity of the conclusions.

and **5**, which both contain 20 carbon lipid chains, have the lowest K_ms and that the turnover numbers are similar for all substrates except **2**, which turns over 10-fold more slowly than the others. Taken together, these data indicate that TagA is sensitive to lipid length/hydrophobicity but not sensitive to lipid structure (branched or unbranched; saturated or unsaturated) or double bond geometry.

Selection of Substrate for Kinetic Studies. The substrate comparison described above shows that compound **5** is preferred to **1**, **2**, and **3**. Nevertheless, initial attempts to use **5** for more detailed kinetic studies of TagA were hampered by substrate inhibition at concentrations above 300 μM. To determine if substrate inhibition correlates with aggregation, we measured the critical micelle concentrations (CMCs) of **4** and **5**, which both show substrate inhibition, and of **1**, which shows no obvious inhibition at the concentrations tested. CMCs were determined using dye-binding (*18*) and surface tension (drop weight) methods (data not shown) (*19*, *20*). None of the substrates formed micelles in the reaction buffer up to 600 μM, the highest concentration tested. We have concluded that none of the substrates aggregate at the concentrations used and that the observed substrate inhibition is a result of inhibitory interactions of these substrates with TagA. To enable kinetic studies of the enzyme over a broad range of substrate concentrations, we decided to use compound **3** as the acceptor substrate because it shows no inhibition at the working concentrations.

Initial Rate Analysis for TagA. Having identified an appropriate acceptor substrate and conditions for kinetic studies of TagA, we carried out initial velocity measurements to determine whether the enzyme follows a sequential or a ping-pong kinetic mechanism. A 5 × 5 matrix of reactions was carried out with UDP-ManNAc and lipid I analogue **3** at varying concentrations. To determine the reaction rate, formation of UDP was monitored by HPLC. Double reciprocal plots of the initial rate data are shown in Figure 5A. The lines in the double reciprocal plots converge, implying that the enzyme utilizes a sequential mechanism in which both substrates bind prior to product release. The slope replot does not pass through the origin, indicating that the mechanism is not a rapid equilibrium ordered mechanism (Figure 5B). Kinetic parameters for TagA based on the initial rate measurements were obtained by fitting the data to the appropriate rate equation after establishing the kinetic mechanism, as described below.

Product Inhibition Analysis. To understand sequential enzymes, it is important to know whether the substrates bind in a compulsory order and, if so, to determine which substrate binds first. Information on substrate binding order provides insight into the catalytic mechanism, can influence the design of high-throughput screens (*21*), and can facilitate efforts to obtain cocrystals with substrate bound (*22*). Product inhibitors yield distinct inhibition patterns depending on the kinetic mechanism of an enzyme and can be used to elucidate the order of substrate binding (see Supporting Information).

To carry out a product inhibition analysis using UDP, we needed an assay that does not rely on detection of UDP.

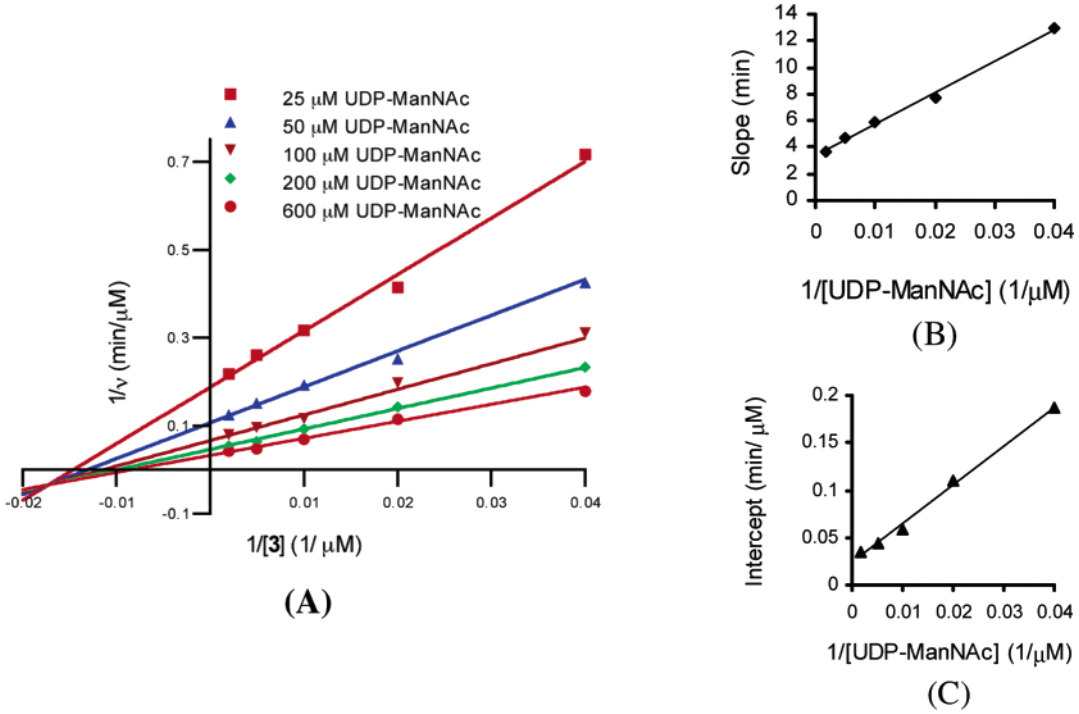

FIGURE 5: (A) Double reciprocal plots of the initial velocity data with respect to **3** as the varied substrate. Initial velocities were measured at the indicated fixed UDP-ManNAc concentrations. Assays were carried out with [UDP-ManNAc] at 25−600 μM, [**3**] at 25−500 μM, and 52 nM TagA. The data were fit to eq 2. (B) Secondary plot of slope vs 1/[UDP-ManNAc]. (C) Secondary plot of intercept vs 1/[UDP-ManNAc].

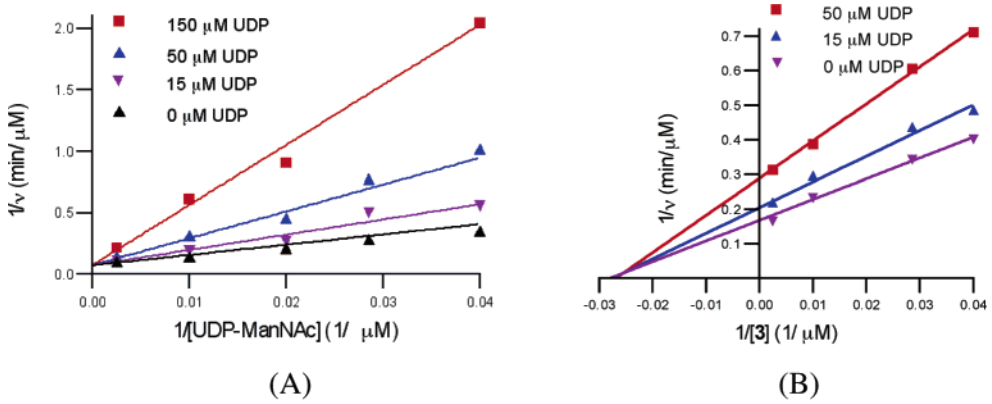

FIGURE 6: (A) Product inhibition by UDP vs UDP-ManNAc. Initial rates were measured at 52 nM TagA and 100 μM **3** in the presence of several fixed concentrations of UDP (0, 15, 50, and 150 μM) and varied UDP-ManNAc (25−400 μM). The data were fit to eq 3 for competitive inhibition. (B) Inhibition of UDP vs lipid I analogue **3**. Initial rates were measured at 52 nM TagA and 100 μM UDP-ManNAc in the presence of several fixed concentrations of UDP (0, 15, and 50 μM) and varied lipid I analogue **3** (25−400 μM). The data were fit to eq 4 for noncompetitive inhibition.

Therefore, we used an LC/MS assay to monitor formation of the other product, lipid II. This assay was adapted from a broadly applicable ESI-MS assay developed by Leary and co-workers, which has been used for kinetic analysis and substrate specificity evaluation of several enzymes, including glutathione *S*-transferase (*23*), hexokinase (*24*), phosphoglucomutase (*25*), and NodH sulfotransferase (*26*, *27*). A similar ESI-MS assay was developed by Pohl and co-workers for kinetic analysis of nucleotidyltransferases (*28*). Ionization can vary from sample to sample, so for accurate product quantitation each sample is doped with an internal standard. We used **4** as an internal standard and to construct a calibration curve for product quantitation. With UDP as a product inhibitor, a competitive inhibition pattern with respect to UDP-ManNAc (Figure 6A) and a noncompetitive inhibition pattern (Figure 6B) with respect to the acceptor **3** were obtained at nonsaturating levels of the fixed substrate. This inhibition pattern ruled out a steady-state ordered Bi-Bi mechanism in which the acceptor binds first, but left several other possibilities (see Supporting Information). To distinguish between these possibilities, we next evaluated the inhibition patterns obtained using lipid II analogues as product inhibitors.

Preliminary experiments showed that the IC_{50} value of lipid II analogue **3a** (Figure 4) was higher than 1 mM when **3** was used as the acceptor (data not shown). By comparison, the IC_{50} value of lipid II analogue **5a** (Figure 4) with respect to **3** was ~15 μM (data not shown). Therefore, product inhib-

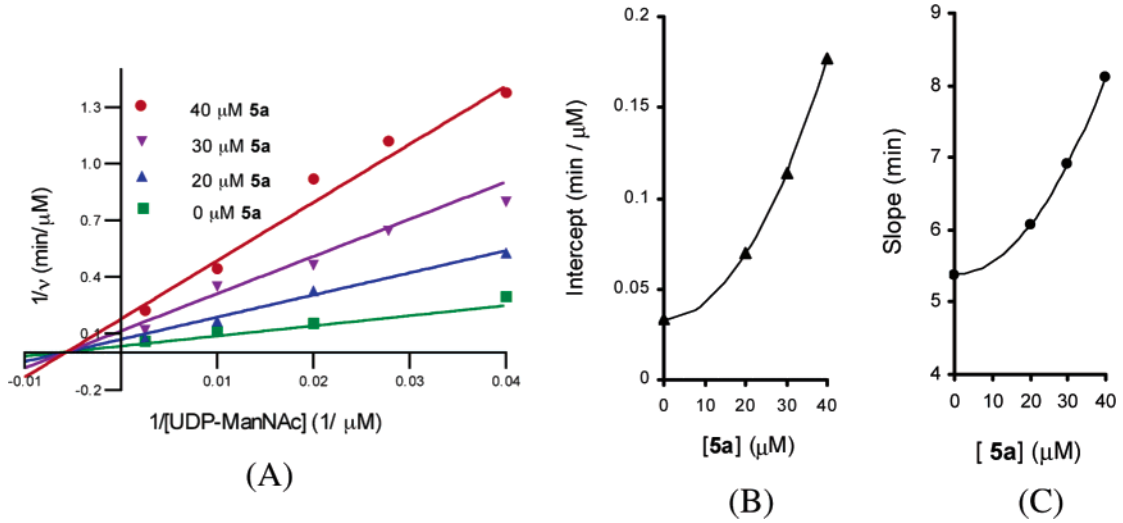

FIGURE 7: (A) Product inhibition by lipid II analogue **5a** vs UDP-ManNAc. Initial rates were measured at 52 nM TagA and 200 μM **3** in the presence of several fixed concentrations of lipid II analogue **5a** (0, 20, 30, and 40 μM) and varied UDP-ManNAc (25−400 μM). The data were fit to eq 5 for *I*-parabolic *S*-parabolic noncompetitive inhibition. (B) Secondary plot of intercept vs [**5a**]. (C) Secondary plot of intercept slope vs [**5a**].

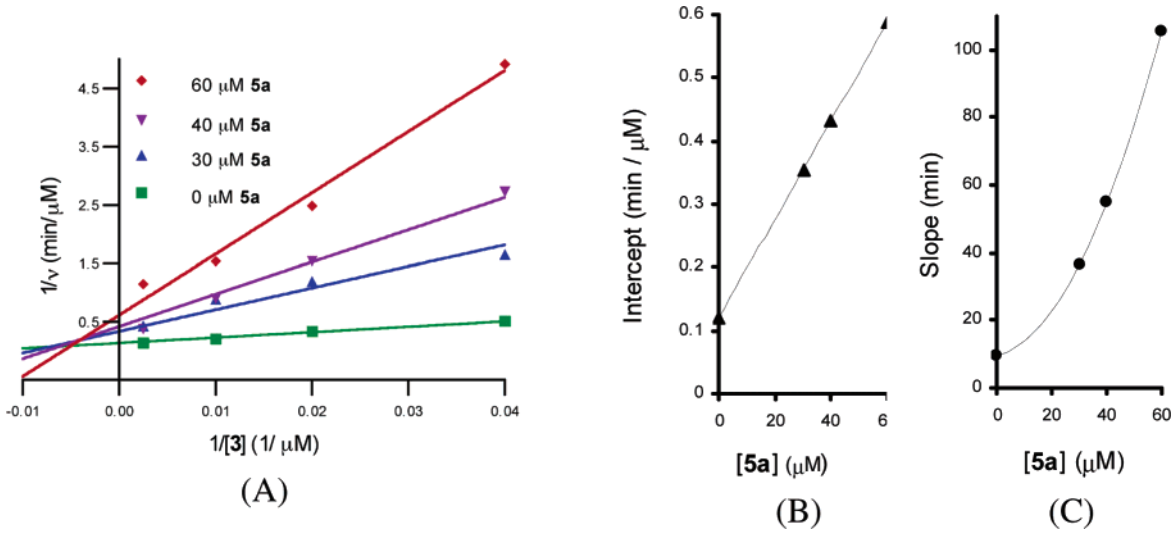

FIGURE 8: (A) Product inhibition by lipid II analogue **5a** vs **3**. Initial rates were measured at 52 nM TagA and 100 μM UDP-ManNAc in the presence of several fixed concentrations of **5a** (0, 30, 40, and 60 μM) and varied **3** (25−400 μM). The data were fit to eq 6 for *I*-linear *S*-parabolic noncompetitive inhibition. (B) Secondary plot of intercept vs [**5a**]. (C) Secondary plot of intercept slope vs [**5a**].

Scheme 1: Steady-State Ordered Bi-Bi Mechanism with Two Dead-End Complexes

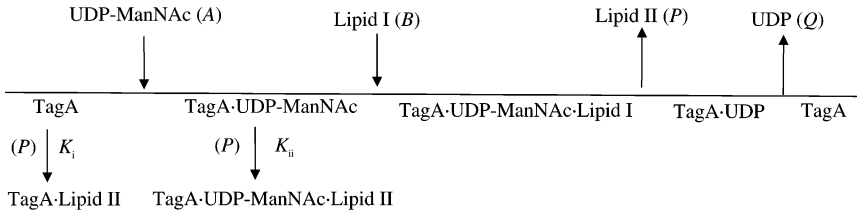

ition experiments were performed using the **3**/**5a** acceptor/product pair. Reactions were monitored using the HPLC assay, which detects the formation of UDP. Product **5a** proved to be an *I*-parabolic, *S*-parabolic noncompetitive inhibitor with respect to UDP-ManNAc (Figure 7A) and an *I*-linear, *S*-parabolic noncompetitive inhibitor (Figure 8A) with respect to the acceptor **3** at nonsaturating levels. These inhibition patterns are consistent with an ordered Bi-Bi mechanism in which the UDP-ManNAc donor binds first and the UDP product is released last (see Supporting Information).

The nonlinear noncompetitive patterns suggest that the product **5a** may exist in more than one enzymatic complex. Given that substrate inhibition was observed when **5** was the acceptor and that **5** and **5a** are similar in structure, we propose that there are two dead-end complexes, TagA·lipid II (EP) and TagA·UDP-ManNAc·lipid II (EAP), involved in the reaction mechanism (Scheme 1). The denominator terms multiplied by $(1 + P/K_i)$ and $(1 + P/K_{ii})$ correspond to the relative concentrations of TagA (E) and the TagA·UDP-ManNAc (EA) complex, respectively. Consequently, the initial rate equation in the presence of *P*

for the ordered Bi-Bi mechanism is

$$v = VAB / \left[K_{ia}K_b\left(1+\frac{P}{K_i}\right) + K_b\left(1+\frac{P}{K_{ii}}\right)A + K_a\left(1+\frac{P}{K_i}\right)B + AB + \frac{K_qK_bK_{ia}}{K_{iq}K_p}\left(1+\frac{P}{K_i}\right)P + \frac{K_qK_b}{K_{iq}K_p}\left(1+\frac{P}{K_{ii}}\right)AP + \frac{1}{K_{ip}}ABP\right]$$

or, in the reciprocal forms:

$$\frac{1}{v} = \frac{1}{V}\left[1+\left(1+\frac{P}{K_{ii}}\right)\left(\frac{K_b}{B}+\frac{K_qK_bP}{K_{iq}K_pB}\right)+\frac{P}{K_{ip}}\right] + \frac{1}{V}\left[\left(1+\frac{P}{K_i}\right)\left(\frac{K_{ia}K_b}{B}+K_a+\frac{PK_qK_bK_{ia}}{K_{iq}K_pB}\right)\right]\frac{1}{A} \quad (7)$$

$$\frac{1}{v} = \frac{1}{V}\left[1+\frac{K_a}{A}\left(1+\frac{P}{K_i}\right)+\frac{P}{K_{ip}}\right] + \frac{1}{V}\left[\frac{K_{ia}K_b}{A}\left(1+\frac{P}{K_i}\right)\left(1+\frac{K_qP}{K_{iq}K_p}\right)+\left(1+\frac{P}{K_{ii}}\right)\left(K_b+\frac{PK_qK_b}{K_{iq}K_p}\right)\right]\frac{1}{B} \quad (8)$$

A and *B* are reactant concentrations and *P* is the product concentration; v and V represent initial and maximum velocities, respectively; K_a, K_b, K_p, and K_q are Michaelis constants for *A*, *B*, *P*, and *Q*; K_{ia}, K_{ip}, and K_{iq} are inhibition constants for *A*, *P*, and *Q*; K_i and K_{ii} are the dissociation constants of the product from the dead-end TagA·lipid II (EP) and TagA·UDP-ManNAc·lipid II (EAP) complexes, respectively.

When *A* (UDP-ManNAc) is varied, the resulting P^2 term appears in the intercept$_{1/A}$ and slope$_{1/A}$ functions, consistent with the *I*-parabolic, *S*-parabolic noncompetitive pattern (Figure 7B,C); when *B* (lipid I) is the varied substrate, the resulting P^2 term only appears in the slope$_{1/B}$ function, in agreement with the *I*-linear, *S*-parabolic noncompetitive pattern (Figure 8B,C).

Taken together, these data imply an ordered Bi-Bi mechanism where UDP-ManNAc binds first and UDP is released last. To obtain the kinetic parameters for the enzyme, the initial rate data from the 5 × 5 matrix described earlier were fit to eq 8 for the determined mechanism. Since initial rate data were used, the product terms in the equation were set to 0. This fit yielded the following values: $k_{cat} = 735 \pm 129$ min^{-1}, $K_a = 154.2 \pm 33.9$ μM, $K_b = 133.1 \pm 30.2$ μM, and $K_{ia} = 67.2 \pm 6.9$ μM (A = UDP-ManNAc; B = lipid I analogue **3**).

DISCUSSION

TagA is involved in a biosynthetic pathway that is a potential target for antimicrobial intervention. Previous mechanistic studies of this enzyme have been hampered by the fact that the natural acceptor for the enzyme contains a 55 carbon undecaprenyl chain. This substrate is anchored in the bacterial membrane, and TagA is believed to be peripherally associated with the membrane. We have previously demonstrated, however, that TagA is active following purification away from bacterial membranes and accepts an artificial substrate containing a short lipid chain. Here, we have expanded on our earlier work, exploring the extent to which TagA recognizes features of the natural lipid chain. Our results show that TagA is moderately sensitive to the length of the lipid but not sensitive to its structure. Thus, the catalytic efficiencies of substrates of equivalent length are almost identical, regardless of unsaturation, branching, or double bond geometry. The demonstrated insensitivity of TagA even to features of the lipid close to the diphosphate linkage at the reducing end of the substrate is consistent with early reports showing that enzymes in the *tag* pathway are able to utilize substrates containing dolichol rather than undecaprenyl chains (*6*).

We report here that the examined substrates containing the longest lipid chains (**4** and **5**) have the highest catalytic efficiencies, showing that lipid length is an important variable in activity. These substrates, however, also display substrate inhibition. We measured the CMCs (critical micelle concentrations) of the substrates in order to determine whether their high catalytic efficiencies or their inhibitory behavior could be attributed to the formation of micellar aggregates. Our results show that these substrates do not form micelles at concentrations up to 600 μM, well above the concentrations at which substrate inhibition is observed. Previously reported data are consistent with our findings, showing that the CMCs of related compounds are in the millimolar range (*29*). Therefore, neither the catalytic efficiencies nor the inhibitory behavior of these substrates results from aggregation. Since the increased catalytic efficiencies of **4** and **5** relative to **2** and **3** are largely due to a decrease in K_m values, we have concluded that the tetraprenyl substrates are more efficient than shorter chain substrates because the longer lipids make more favorable hydrophobic interactions with TagA.

The severe substrate inhibition observed with the longer chain substrates may arise because there is a structural resemblance between the acceptor and the donor. That is, the acceptor contains a diphospho-GlcNAc moiety whereas the donor contains a diphospho-ManNAc moiety. The synthetic acceptors with the longer lipid chains may be able to establish sufficiently favorable hydrophobic interactions that they bind stably in the donor site. Consistent with this hypothesis, we have found that inhibition by these acceptor substrates is dependent on the donor sugar concentration (data not shown).

On the basis of information about the behavior of the different artificial substrates, we selected a substrate/product pair with suitable properties for a kinetic analysis. Using a product inhibition analysis, we have shown that TagA uses an ordered Bi-Bi mechanism in which UDP-ManNAc binds first and UDP is released last. The turnover number for the enzyme, obtained from a 5 × 5 matrix of reactions, was found to be 735 min^{-1}, which is relatively fast and consistent with the function of this enzyme in a primary metabolic pathway. The K_m for UDP-ManNAc is also reasonable given estimated concentrations of this substrate in cells. We do not think it is possible to draw any conclusions about the K_m of the natural acceptor substrate from the K_m measured for the synthetic substrates used in these studies because of

the differences in presentation; that is, the natural substrate is anchored in a membrane while the synthetic analogues are not. Nevertheless, these studies have conclusively established that TagA does *not* require biological membranes or a micellar interface to function well. They have also provided information on acceptor substrates that may be useful tools in further kinetic studies of TagA. It should be possible, for example, to use these substrates to analyze mutants of TagA to probe the roles of various amino acids. Finally, we note that information on the kinetic mechanism of TagA should simplify efforts to obtain crystals of the enzyme with substrates bound and may also influence the design of high-throughput assays for inhibitors.

We note in closing that the glycosylation reaction catalyzed by TagA—the transfer of a sugar from a nucleotide sugar donor to a lipid-linked monosaccharide acceptor—is not unique. Analogous reactions are performed by many enzymes, including other CAZy family 26 members as well as the second enzyme in the eukaryotic dolichol pathway for N-linked glycosylation (*30*) and MurG (*14*, *22*, *31*), which is involved in the biosynthesis of peptidoglycan. MurG and the second enzyme in the dolichol pathway are members of the GT-B superfamily of glycosyltransferases (*11*−*14*), which consist of two Rossmann domains, one containing a signature nucleotide-binding motif. TagA does not appear to belong to the GT-B superfamily because it is substantially shorter than these enzymes and lacks the nucleotide binding motif. It also bears little resemblance to characterized enzymes of the GT-A superfamily, the other major glycosyltransferase fold family. These enzymes have an absolute requirement for a Mg^{2+} or Mn^{2+} cation, which chelates the nucleotide−sugar in the active site. Although TagA is predicted to be an α/β protein like the GT-A superfamily members, threading analysis suggests that it does not have the same fold (*11*), and the experiments reported here show that it does not require metal ions for activity. TagA and its relatives in CAZy family 26 (*8*) may represent a new fold variant, and the studies reported here suggest that TagA is a particularly promising model system for understanding CAZy family 26. Efforts to crystallize TagA are currently underway.

ACKNOWLEDGMENT

We thank Dr. David Rudner for providing purified *B. subtilis* PY79 genomic DNA.

SUPPORTING INFORMATION AVAILABLE

Michaelis−Menten plots of **1**−**5**, the effect of pH and DMSO on TagA activity, and a table of expected product inhibition patterns for selected ordered and random Bi-Bi kinetic mechanisms. This material is available free of charge via the Internet at http://pubs.acs.org.

REFERENCES

1. Neuhaus, F. C., and Baddiley, J. (2003) A continuum of anionic charge: structures and functions of D-alanyl-teichoic acids in Gram-positive bacteria, *Microbiol. Mol. Biol. Rev. 67*, 686−723.
2. Bhavsar, A. P., Erdman, L. K., Schertzer, J. W., and Brown, E. D. (2004) Teichoic acid is an essential polymer in *Bacillus subtilis* that is functionally distinct from teichuronic acid, *J. Bacteriol. 186*, 7865−7873.
3. Kobayashi, K., Ehrlich, S. D., Albertini, A., Amati, G., Andersen, K. K., Arnaud, M., Asai, K., Ashikaga, S., Aymerich, S., Bessieres, P., et al. (2003) Essential *Bacillus subtilis* genes, *Proc. Natl. Acad. Sci. U.S.A. 100*, 4678−4683.
4. Weidenmaier, C., Peschel, A., Xiong, Y. Q., Kristian, S. A., Dietz, K., Yeaman, M. R., and Bayer, A. S. (2005) Lack of wall teichoic acids in *Staphylococcus aureus* leads to reduced interactions with endothelial cells and to attenuated virulence in a rabbit model of endocarditis, *J. Infect. Dis. 191*, 1771−1777.
5. Weidenmaier, C., Kokai-Kun, J. F., Kristian, S. A., Chanturiya, T., Kalbacher, H., Gross, M., Nicholson, G., Neumeister, B., Mond, J. J., and Peschel, A. (2004) Role of teichoic acids in *Staphylococcus aureus* nasal colonization, a major risk factor in nosocomial infections, *Nat. Med. 10*, 243−245.
6. Yokoyama, K., Mizuguchi, H., Araki, Y., Kaya, S., and Ito, E. (1989) Biosynthesis of linkage units for teichoic acids in Gram-positive bacteria: distribution of related enzymes and their specificities for UDP-sugars and lipid-linked intermediates, *J. Bacteriol. 171*, 940−946.
7. Soldo, B., Lazarevic, V., and Karamata, D. (2002) *TagO* is involved in the synthesis of all anionic cell-wall polymers in *Bacillus subtilis* 168, *Microbiology 148* (Part 7), 2079−2087.
8. Coutinho, P. M., and Henrissat, B. Carbohydrate-Active Enzymes server (http://www.cazy.org).
9. Erbel, P. J., Barr, K., Gao, N., Gerwig, G. J., Rick, P. D., and Gardner, K. H. (2003) Identification and biosynthesis of cyclic enterobacterial common antigen in *Escherichia coli*, *J. Bacteriol. 185*, 1995−2004.
10. Haft, R. F., Wessels, M. R., Mebane, M. F., Conaty, N., and Rubens, C. E. (1996) Characterization of *cpsF* and its product CMP-*N*-acetylneuraminic acid synthetase, a group B streptococcal enzyme that can function in K1 capsular polysaccharide biosynthesis in *Escherichia coli*, *Mol. Microbiol. 19*, 555−563.
11. Breton, C., Snajdrova, L., Jeanneau, C., Koca, J., and Imberty, A. (2006) Structures and mechanisms of glycosyltransferases, *Glycobiology 16*, 29R−37R.
12. Rosen, M. L., Edman, M., Sjostrom, M., and Wieslander, A. (2004) Recognition of fold and sugar linkage for glycosyltransferases by multivariate sequence analysis, *J. Biol. Chem. 279*, 38683−38692.
13. Ünligil, U. M., and Rini, J. M. (2000) Glycosyltransferases structure and mechanism, *Curr. Opin. Struct. Biol. 1*, 510−517.
14. Hu, Y., and Walker, S. (2002) Remarkable structural similarities between diverse glycosyltransferases, *Chem. Biol. 9*, 1287−1296.
15. Ginsberg, C., Zhang, Y.-H., Yuan, Y., and Walker, S. (2006) *In vitro* reconstitution of two essential steps in wall teichoic acid biosynthesis using synthetic substrate analogs, *ACS Chem. Biol. 1*, 25−28.
16. Zahn, T. J., Whitney, J., Weinbaum C., and Gibbs, R. A. (2001) Synthesis and evaluation of GGPP geometric isomers: divergent substrate specificities of FTase and GGTase I, *Bioorg. Med. Chem. Lett. 11*, 1605−1608.
17. Xie, H., Shao, Y., Becker, J. M., Naider, F., and Gibbs, R. A. (2000) Synthesis and biological evaluation of the geometric farnesylated analogs of the a-factor mating peptide of *Saccharomyces cerevisiae*, *J. Org. Chem. 65*, 8552−8563.
18. Ananthapadmanabhan, K. P., Goddard, E. D., Turro, N. J., and Kuo, P. L. (1985) Fluorescence probes for critical micelle concentration, *Langmuir 1*, 352−355.
19. Yildirim, O. E., Xu, Q., and Basaran, O. A. (2005) Analysis of the drop weight method, *Phys. Fluid 17*, 062107/1−062107/13.
20. Jho, C., and Burke, R. J. (1983) Drop weight technique for the measurement of dynamic surface tension, *J. Colloid Interface Sci. 95*, 61−71.
21. Helm, J. S., Hu, Y., Chen, L., Gross, B., and Walker, S. (2003) Identification of active-site inhibitors of MurG using a generalizable, high-throughput glycosyltransferase screen, *J. Am. Chem. Soc. 125*, 11168−11169.
22. Hu, Y., Chen, L., Ha, S., Gross, B., Falcone, B., Walker, D., Mokhtarzadeh, M., and Walker, S. (2003) Crystal structure of the MurG: UDP-GlcNAc complex reveals common structural principles of a superfamily of glycosyltransferases, *Proc. Natl. Acad. Sci. U.S.A. 100*, 845−849.
23. Ge, X., Sirich, T. L., Beyer, M. K., Desaire, H., and Leary, J. A. (2001) A strategy for the determination of enzyme kinetics using electrospray ionization with an ion trap mass spectrometer, *Anal. Chem. 73*, 5078−5082.

24. Gao, H., and Leary, J. A. (2003) Multiplex inhibitor screening and kinetic constant determinations for yeast hexokinase using mass spectrometry based assays, *J. Am. Soc. Mass Spectrom. 14*, 173−181.
25. Gao, H., and Leary, J. A. (2004) Kinetic measurements of phosphoglucomutase by direct analysis of glucose-1-phosphate and glucose-6-phosphate using ion/molecule reactions and Fourier transform ion cyclotron resonance mass spectrometry, *Anal. Biochem. 329*, 269−275.
26. Pi, N., Armstrong, J. I., Bertozzi, C. R., and Leary, J. A. (2002) Kinetic analysis of NodST sulfotransferase using an electrospray ionization mass spectrometry assay, *Biochemistry 41*, 13283−13288.
27. Pi, N., Yu, Y., Mougous, J. D., and Leary, J. A. (2004) Observation of a hybrid random ping-pong mechanism of catalysis for NodST: a mass spectrometry approach, *Protein Sci. 13*, 903−912.
28. Zea, C. J., and Pohl, N. L. (2004) General assay for sugar nucleotidyltransferases using electrospray ionization mass spectrometry, *Anal. Biochem. 328*, 196−202.
29. Visscher, I. (2004) Amphiphiles containing aromatic groups in the hydrophobic part, Ph.D. Thesis, Chapter 2, pp 21−33 (http://irs.ub.rug.nl/ppn/269298355).
30. Chantret, I., Dancourt, J., Barbat, A., and Moore, S. E. (2005) Two proteins homologous to the N-and C-terminal domains of the bacterial glycosyltransferase MurG are required for the second step of dolichyl-linked oligosaccharide synthesis in *Saccharomyces cerevisiae*, *J. Biol. Chem. 280*, 9236−9242.
31. Ha, S., Walker, D., Shi, Y., and Walker, S. (2000) The 1.9 Å crystal structure of *Escherichia coli* MurG, a membrane-associated glycosyltransferase involved in peptidoglycan biosynthesis, *Protein Sci. 9*, 1045−1052.

BI060872Z